IEEE Access
Multidisciplinary | Rapid Review | Open Access Journal

Received May 8, 2019, accepted June 25, 2019, date of publication July 11, 2019, date of current version July 24, 2019.

Digital Object Identifier 10.1109/ACCESS.2019.2927033

The Applications of Compliant Motion Control Technique on 6-DOF Hydraulic Parallel Mechanism

SHUPENG ZHENG[1], CHANGHONG GAO[2], XINJIAN NIU[3], DACHENG CONG[3], AND JUNWEI HAN[3]

[1]School of Electrical and Information, Northeast Agricultural University, Harbin 150030, China
[2]Aviation Equipment Research Institute, AVIC Qing'an Group Company Ltd., Xi'an 710003, China
[3]State Key Laboratory of Robotics and System, Harbin Institute of Technology, Harbin 150001, China

Corresponding author: Shupeng Zheng (zheng_sp@126.com)

ABSTRACT Most interaction control formulations focused on electrically driven parallel mechanism. In this paper, the combining practice applications of compliant motion control technique on six degrees of freedom (6-DOF) hydraulic parallel mechanism (HPM) are investigated. According to the manipulation task specification and hydraulic control system characteristics, three different compliant motion control schemes are presented in three typical application scenarios, respectively: a parallel position/force control scheme in the joint space coordinate for train curve negotiation performance test, a hybrid position/force control scheme with the internal force suppression for shaking table with actuation redundancy, and a hybrid impedance control scheme for auto-docking mechanism based on force and vision. The feasibility and effectiveness of the proposed schemes were verified through a series of experiments. It showed that the 6-DOF HPM achieves good compliant behavior by applying the proposed compliant motion control techniques. These schemes could also be extended to other applications where the compliant motion of the 6-DOF HPM is required.

INDEX TERMS Compliant motion control, force control, interaction control, hydraulic parallel mechanism, hydraulic control system.

I. INTRODUCTION

Interaction control [1]–[3] is an important technology for applying robot to many engineering domains, such as fastening screw, flight-refuel, and object contour surface tracking, etc. When contacting, the end-effector is subject to environmental constraints, moving along directions in the specific task space, and the compliance characteristics are needed. The compliant behavior can be achieved in passive or active mode [4]. In the passive mode, the trajectory of end-effector is corrected by the contact force due to the compliant mechanism of the manipulator. There is no need for force sensors and this approach is relatively simple and inexpensive. However, the use of passive compliance lacks flexibility because of the low versatility of the compliant mechanism for different operating conditions. The alternative is active compliant motion control, where the control system could react to force and can be easily modified to adapt different interaction conditions.

Many active compliant motion control schemes have been studied by Whitney [5], Zeng and Hemami [6]. Three typical control schemes are impedance control, hybrid control and parallel control. Impedance control [7] devotes to build the connection between the contact force and the position of end-effector without controlling force explicitly. Hybrid control [8] divides the task space into degrees of freedom (DOF) and merely control position or force. Parallel control [9] can simultaneously control position and force by using position and force controller in parallel. The implementation and performance comparison of aforementioned control schemes have been carried out on a serial industrial robot by Chiaverini *et al.* [10]. Moreover, many extended approaches such as external control [11], hybrid impedance control [12] and fuzzy adaptive control [13], [14] have also been proposed.

The 6-DOF parallel mechanism (PM) is widely applied in interaction task by virtues of higher force capabilities,

The associate editor coordinating the review of this manuscript and approving it for publication was Huanqing Wang.

lower inertia, and higher stiffness than serial mechanism [16]. Recently, a lot of compliant motion control techniques were proposed for 6-DOF parallel mechanism. However, most of studies focused on the electrically driven PM where the output torque of the electric actuator has linear relation with the driver current. In this case, the compliant motion control is easily implemented with the knowledge of dynamics and kinematics of the PM. In many applications, the hydraulic parallel mechanism is always more preferred than electrically driven PM because the hydraulic system has higher precision, faster response speed and more payload capability with relatively low mass and size. Unfortunately, it is difficult to apply similar methods on hydraulic servosystem due to following two challenges [17], [18]. The first challenge arises from the inherent high nonlinearities of hydraulic servosystem, e.g., the position dependence of the actuator dynamics and the flow load sensitivity of hydraulic servo valve. The second challenge arises from the small damping of hydraulic servosystem, e.g., the low zero flow-pressure coefficient of hydraulic servo valve and the leakage of hydraulic actuator.

There are few reports on the compliant motion control of hydraulic parallel mechanisms (HPM). By using the 6-DOF HPM, A force/position control algorithm with model-based actuators' forces fuzzy compensation was implemented for the multi-directional assembly of tunnel segments [19]. However, the design of fuzzy logic rule base and inference directly determines the control performance. It is generally difficult and often depends on experiences [20]. A compliant motion control scheme with compensations for interaction force control and positional error recovery was proposed for a 6-DOF HPM and has been used for surgical operation [21]. However, the implemented inverse dynamics model does not consider the detailed actuator dynamics.

In this paper, the combining practice application of compliant motion control techniques on 6-DOF HPM are investigated. Three different compliant motion control schemes were presented in three typical application scenarios, respectively.

The first application is the train carriage end relationship integrated test rig which composes of a 6-DOF HPM, a horizontally fixed hydraulic actuator and an articulated equipment. The 6-DOF HPM and the horizontally fixed hydraulic actuator coordinate their movements to fulfill the maximum swing angle requirement of the articulated equipment. In order to reduce the stiffness of the position loop and achieve the compliant behavior, a parallel position/force control scheme was proposed on the basis of joint space control scheme. Furthermore, the dynamic force feedback with a high-pass filter was used to increase the damping of hydraulic servosystem without reducing stiffness.

The second application is the shaking table with actuation redundancy which composes of a 6-DOF HPM and two actuation redundancies. In order to guarantee the safety of the mechanism and improve the control performance of the system, the internal-force of the hydraulically redundant actuated parallel mechanism should be suppressed. To this end, a hybrid position/force control scheme was proposed on the basis of the internal force space analysis. Furthermore, an acceleration feedback loop was introduced to increase the damping of hydraulic servosystem and improve the bandwidth of pose tracking.

The third application is an auto-docking mechanism which composes of a 6-DOF HPM, the target object and the vision system. In order to enhance the dexterity and guarantee the safety of interaction task, a hybrid impedance control scheme was proposed on the basis of vision and force. Furthermore, the dynamic pressure feedback and a nonlinear compensation module were introduced to increase the damping of hydraulic system and overcome the negative impacts of flow load sensitivity of hydraulic servo valve on control system respectively.

The remainder of this paper is organized as follows. Section II describes the system configuration of the first application, presents the parallel position/force control scheme and verifies the proposed control scheme by train curve negotiation performance test. Section III describes the system configuration of the second application, presents the hybrid position/force control scheme and verifies the proposed control scheme by vibration test. The system configuration, control scheme and experiment results of the third application are given in Section IV. Finally, conclusion is drawn in Section V.

II. TRAIN CARRIAGE END RELATIONSHIP INTEGRATED TEST RIG

A. SYSTEM DESCRIPTION

The train carriage end relationship integrated test rig is used to carry out motion interference test, function test and research test of the train carriage end components. It can also realize motion simulation and force loading with a high precision.

Fig. 1 is the system configuration of the test rig. A 6-DOF HPM is horizontally fixed on the base plate with hooke joints which composes of six hydraulic actuators and a simulated carriage end. Each hydraulic actuator consists of an asymmetric servo valve and an asymmetric hydraulic cylinder. A force sensor is installed between the piston rod and the upper joint. The articulated equipment installed between two simulated

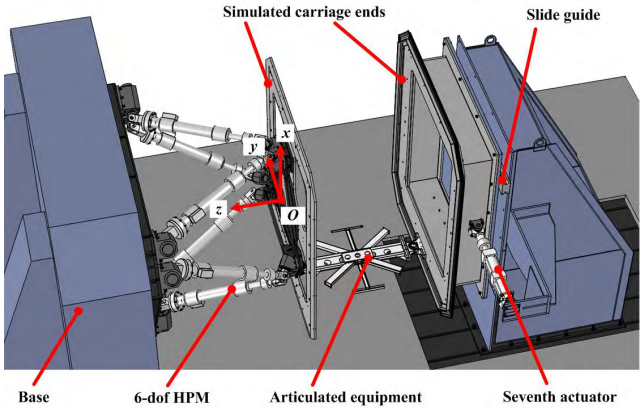

FIGURE 1. Train carriage end relationship integrated test rig.

train carriage ends is used to carry out the curve negotiation performance test. During testing, the 6-DOF HPM is required to move horizontally with the articulated equipment to simulate the relative motion of the train carriage ends in horizontal plane. The maximum swing angle of the articulated equipment is up to 35°. To this end, in coordination with the 6-DOF HPM, an additional hydraulic actuator (the seventh actuator) is used to push one simulated carriage end horizontally along the slide guides in y direction.

B. SYSTEM FEATURES AND CONTROL SCHEME

The test rig has two significant features. First, the articulated equipment is connected with the simulated carriage ends by revolute joints which is the rigid part. During moving, pure position control which relies entirely on task planning and the exact dynamics model, will inevitably generate large contact force. In order to guarantee the safety of the articulated equipment, the contact force should be well controlled. Accordingly, the compliant behavior of the 6-DOF HPM is required. Second, there is no six-dimensional force sensor in the system. The system only has a force sensor for each hydraulic actuator to measure the axial force. However, the compliant motion control requires three translational forces and three torques to offer the complete contact force information. Therefore, the force information of each hydraulic actuator should be fully utilized to achieve the required compliant behavior.

In view of above features, firstly, a parallel position/force control scheme in the joint space coordinate is devised where a force control loop is parallel with the position control loop. The force control loop is extra introduced to make the 6-DOF HPM has good compliant behavior to accommodate the interaction tasks. Then, a position control loop of the seventh actuator with dynamic force feedback is used to control the position of the seventh actuator as accuracy as possible. Finally, the integrated control for the test rig is presented.

1) CONTROL LOOP OF THE 6-DOF HPM

Independent joint space control scheme has been widely applied on motion control of the robot due to its simple structure and light computational load [22]. The joint space control can track the desired motion commands derived from the commands given in task space by using the inverse kinematics.

To achieve the suitable compliant behavior, a parallel position/force control scheme is proposed on the basis of the joint space control scheme. The force control loop is introduced to parallel with the position control loop due to following two purposes. The first one is to increase the damping of hydraulic servosystem so that high position feedback gain can be used to improve the system response. The second is to reduce the stiffness of the position loop so that the compliant behavior can be achieved to accommodate interaction tasks.

As shown in Fig. 2, in the joint space, the desired actuator length vector $\boldsymbol{l}_{d1-6}$ is compared with the feedback actuator length vector $\boldsymbol{l}_{1-6}$ and the resulted actuator length error $\boldsymbol{e}_{lh}$

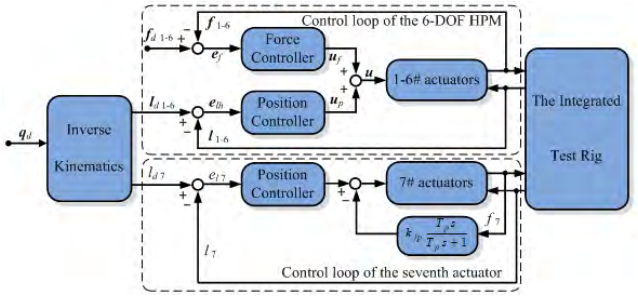

FIGURE 2. Integrated control block diagram for the integrated test rig.

is then fed into the position controller. The desired actuator force vector $\boldsymbol{f}_{d1-6}$ is compared with feedback actuator force vector $\boldsymbol{f}_{1-6}$ and the resulted force error $\boldsymbol{e}_f$ is then fed into the force controller. The final control input $\boldsymbol{u}$ of the servo valves of six hydraulic actuators is the combination of the force loop control output quantities $\boldsymbol{u}_f$ and the position loop control output quantities $\boldsymbol{u}_p$. The proportional controllers are used for both position control and force control loop. Therefore, the control law can be expressed as following:

$$\boldsymbol{u} = \boldsymbol{k}_l \boldsymbol{e}_{lh} + \boldsymbol{k}_f \boldsymbol{e}_f \tag{1}$$

where $\boldsymbol{k}_l$ and $\boldsymbol{k}_f$ are 6×6 diagonal proportional gain matrix.

2) CONTROL LOOP OF THE SEVENTH ACTUATOR

In the position control of the seventh actuator, the dynamic force feedback using feedback force with a high-pass filter is applied to increase the damping without reducing stiffness and further improve the bandwidth of control loop. The dynamic force feedback is given by

$$u_{fp} = k_{fp} \frac{T_p s}{T_p s + 1} f_7 \tag{2}$$

where k_{fp} is the dynamic pressure feedback gain, T_p is the time constant, and f_7 is the force feedback of the seventh actuator.

By using PI controller, the control law can be expressed as following:

$$u_7 = k_{P7} e_{l7} + k_{I7} \int_0^t e_{l7} dt - u_{fp} \tag{3}$$

where k_{P7} and k_{I7} are the gain matrix for proportional and integral part respectively, e_{l7} is the seventh actuator length error.

3) INTEGRATED CONTROL

The integrated control strategy for the integrated test rig is shown by Fig. 2. According to the 6×1 desired pose vector $\boldsymbol{q}_d = [\mathrm{x\ y\ z}\ \varphi\theta\psi]^\mathrm{T}$ of the 6-DOF HPM, where the first three variables are translational positions and the last three are attitude angles. The desired actuator length vector $\boldsymbol{l}_{d1-6}$ and the desired actuator length $\boldsymbol{l}_{d7}$ of the seventh actuator could be solved by inverse kinematics. Through using the parallel position/force control loop of the 6-DOF HPM and the position control loop of the seventh actuator, interaction

tasks of the train curve negotiation performance test could be carried out with compliance and the desired commands could also be tracked as accuracy as possible.

C. EXPERIMENT AND RESULTS

A series of train curve negotiation performance test experiments have been performed to verify the effectiveness of the proposed control scheme. In the experiments, the desired position and attitude angle in x direction were both set to zero. The movement path of the 6-DOF HPM in horizontal plane was planned and the desired position of the seventh actuator was derived subsequently to achieve the maximum swing angle (35°) for the articulated equipment. The six desired actuator forces were also set to zero. In the beginning, the platform was located at $x = 0.0$ m, $y = 0.0$ m and $z = 0.23$ m. Then, a sinusoidal motion command with amplitude of 0.51 m and frequency of 0.025 Hz was given in y direction. Meanwhile, a sinusoidal motion command with amplitude of 0.15 m, frequency of 0.05 Hz and phase lag of $\pi/2$ rad was given in z direction.

The motion trajectory of the 6-DOF HPM in yoz plane and the position tracking response of the seventh actuator were shown in Fig. 3(a) and Fig. 3(b) respectively, where the feedback pose of the HPM was computed by forward kinematics solution with Newton-Raphson method [23]. The feedback swing angle of the articulated equipment was derived from the feedback position of the 6-DOF HPM in y and z direction and feedback position of the seventh actuator. It indicated that the position tracking errors of the 6-DOF HPM and the seventh actuator were both small and achieved good accuracy. On the basis of these merits, the angle tracking error of the articulated equipment was small and the maximum swing angle of the articulated equipment (35°) was achieved well, as shown by Fig. 3(c).

In order to justify the benefits of the proposed parallel control scheme, the contact force comparison test was carried out. Initially, a pure position controller was attained for the 6-DOF HPM by removing the force control loop. Then, the parallel control law was applied with the same position loop settings as before and with the force loop gain $\boldsymbol{k}_f = \text{diag}\{0.2\ 0.2\ 0.2\ 0.2\ 0.2\ 0.2\}$. The contact forces in y and z direction were approximately estimated by the feedback force of six actuators. As shown in Fig. 3(d), the contact force in y direction was changing with the angle tracking of the articulated equipment. The bigger swing angle of the articulated equipment was, the greater contact force was, and vice versa. Throughout the test, the contact force with the pure position controller varied over a wide range and the maximum contact force was about -6.5 kN. By contrast, the changes of contact force with the parallel controller were confined to a smaller range. Furthermore, the maximum contact force was reduced to -2.5 kN. The contact force in z direction has similar properties as in y direction, as indicated by Fig. 3(e). In comparison with the pure position controller, the parallel controller reduced the maximum contact force in z direction from 9.6 kN to 5.0 kN.

The experiment results indicated that the proposed parallel position/force control scheme effectively reduces the stiffness of the position loop of the 6-DOF HPM to make it has good compliant behavior. Meanwhile, the position tracking achieves good accuracy. It is feasible and effective to apply the proposed parallel position/force control scheme to the train carriage end relationship integrated test rig.

III. SHAKING TABLE WITH ACTUATION REDUNDANCY

A. SYSTEM DESCRIPTION

Shaking table is an important facility for vibration test, which has been widely used in aviation, automobiles and civil engineering fields, etc. In order to improve the payload of vibration test, hydraulically redundant actuated parallel mechanisms were usually adopted [24]. A 6-DOF HPM with two actuation redundancies (HPM-2AR) for vibration test is shown in Fig. 4. It composes of eight hydraulic actuators and a movement platform, which is fixed on base plates with ball joints. Each hydraulic actuator consists of a symmetrical servo valve, a symmetrical hydraulic cylinder with a built-in displacement sensor and has a differential pressure sensor. An acceleration sensor was installed on each side of the platform and nearby the upper joint of vertical actuators. The size of movement platform is $1.0m \times 1.0m$ and it has large movement range: the bidirectional motion range in horizontal direction is $\pm 0.28m$, the bidirectional motion range in vertical direction is $\pm 0.18m$ and when the horizontal displacement reaches the maximum, the swing angle of vertical hydraulic cylinder was close to 10.0°.

B. SYSTEM FEATURES AND CONTROL SCHEME

The HPM-2AR has two significant features. First, since redundant actuation is adopted, it generates antagonistic actuator forces without external influence. The inconsistence of dynamic characteristics of actuators, zero-drifts of servo valve and uncertainties of geometric model usually produce undesirable internal forces [31]. The large internal forces reduce the control performance of the system and even damage the mechanical parts unless they were balanced. Therefore, suppressing internal-force is also a kind of compliant behavior which should be considered during controller design. Second, the HPM-2AR has relatively large movement range compared to platform size. When the HPM-2AR is moving in a wide range, the movement transformation relationship between the DOF space and the joint space of hydraulic cylinder will change greatly with the platform position. Moreover, the form of internal force space will also change. This scenario may result in large movement errors and worsen the internal force suppression effect.

In view of above features, the internal force space structure of the redundant shaking table was analyzed, firstly. Then, by using the basis of internal force space, a hybrid position/force control scheme was devised which comprises of a position tracking control loop and an internal force suppression control loop. The position tracking control loop is used to

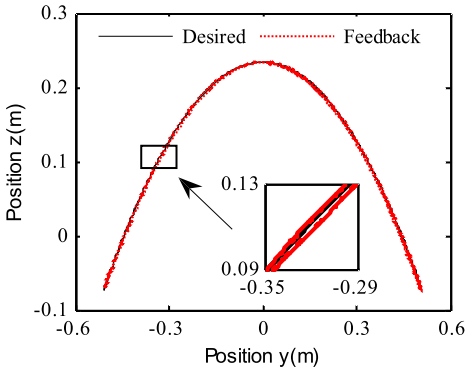

(a) Motion trajectory of the 6-DOF HPM in *yoz* plane.

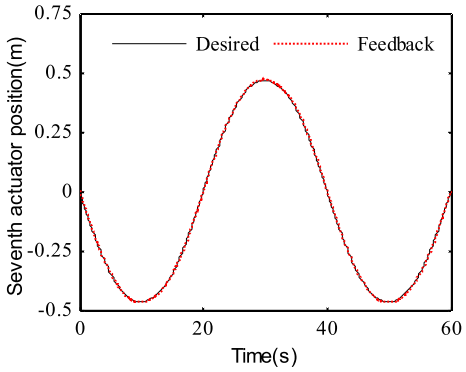

(b) Position tracking response of the seventh actuator.

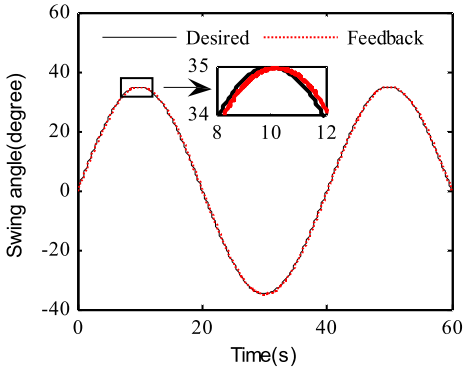

(c) Angle tracking response of the articulated equipment.

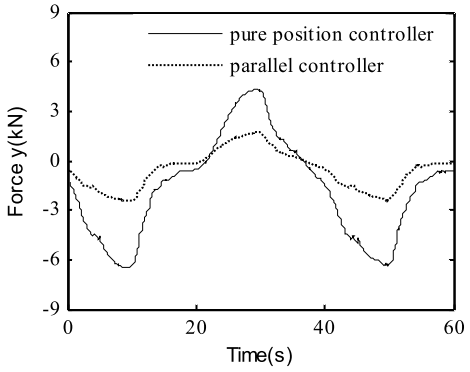

(d) Contact force in *y* direction.

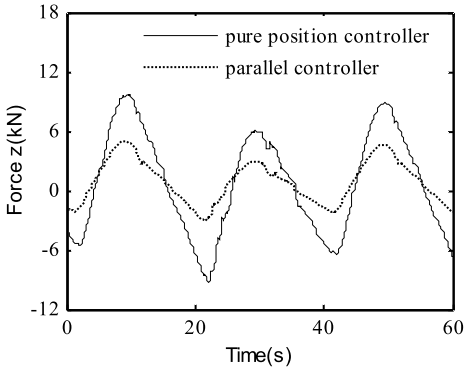

(e) Contact force in *z* direction.

FIGURE 3. **The train curve negotiation performance test results.**

control the movement platform pose as accuracy as possible in the task space. While, the internal force suppression control loop is used to eliminate the internal force caused by the movement of platform. Finally, the integrated control for redundancy shaking table is presented.

1) INTERNAL FORCE SPACE AND DERIVATION OF ITS BASIS

The dynamic equation for HPM-2AR can be simplified as following [25]:

$$\boldsymbol{M}(\boldsymbol{q})\ddot{\boldsymbol{q}} + \boldsymbol{C}(\boldsymbol{q},\dot{\boldsymbol{q}})\dot{\boldsymbol{q}} + \boldsymbol{G}(\boldsymbol{q}) = \boldsymbol{J}(\boldsymbol{q})^{\mathrm{T}} f \ \mathcal{D}\ \boldsymbol{F} \tag{4}$$

where $\boldsymbol{q}$ is the 6×1 vector of the generalized coordinates for movement platform, $\dot{\boldsymbol{q}}$ is the 6×1 vector of the generalized velocity, $\ddot{\boldsymbol{q}}$ is the 6×1 vector of the generalized acceleration, $\boldsymbol{M}(\boldsymbol{q})$ is the 6×6 mass matrix, $\boldsymbol{C}(\boldsymbol{q},\dot{\boldsymbol{q}})$ is the 6×6 centrifugal forces, $\boldsymbol{G}(\boldsymbol{q})$ is the 6×1 vector of gravity, $\boldsymbol{f}$ is the 8×1 vector of actuator forces, $\boldsymbol{F}$ is the 6×1 vector of the generalized forces and $\boldsymbol{J}(\boldsymbol{q})$ is the 8×6 Jacobian matrix which denotes the relationship between generalized velocity and actuator velocity.

The general solution of equation (4) can be expressed as following [25]:

$$f = \left(\boldsymbol{J}^{\mathrm{T}}\right)^{+} \boldsymbol{F}\mathcal{C}\left[I - \left(\boldsymbol{J}^{\mathrm{T}}\right)^{+}\boldsymbol{J}^{\mathrm{T}}\right]\boldsymbol{\lambda} \tag{5}$$

where $\left(\boldsymbol{J}^{\mathrm{T}}\right)^{+}$ is the 8×6 pseudo-inverse matrix of $\boldsymbol{J}^{\mathrm{T}}$, $\mathbf{I}$ is the 8×8 identity matrix, $\boldsymbol{\lambda}$ is the 8×1 freely chosen vector.

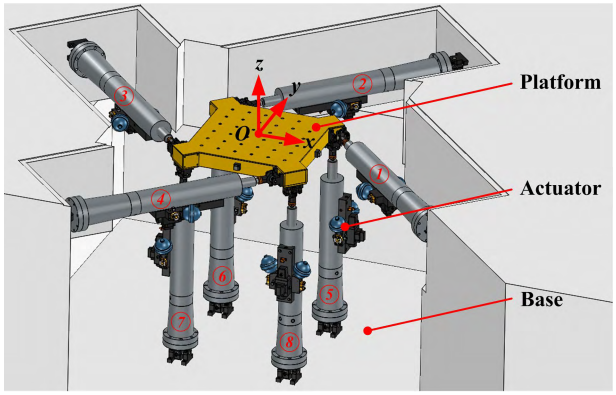

FIGURE 4. Shaking table with two actuation redundancies.

In equation (5), only $\left(\boldsymbol{J}^{\mathrm{T}}\right)^{+}\boldsymbol{F}$ (the particular solution) can effectively resist external load, and $\left[\boldsymbol{I}-\left(\boldsymbol{J}^{\mathrm{T}}\right)^{+}\boldsymbol{J}^{\mathrm{T}}\right]$ (the general solution) is the invalid internal force.

Let $\boldsymbol{S}$ denote internal force space and $\boldsymbol{B}=\boldsymbol{I}-\left(\boldsymbol{J}^{\mathrm{T}}\right)^{+}\boldsymbol{J}^{\mathrm{T}}$ as the matrix of internal force space. The mapping between $\boldsymbol{S}$ and $\boldsymbol{f}$ is expressed as following:

$$\boldsymbol{B}\boldsymbol{f}=\boldsymbol{S} \tag{6}$$

Let 8×2 matrix $\boldsymbol{E}$ denote the basis of internal force space, which is the null-space of matrix $\boldsymbol{J}^{\mathrm{T}}$. Define $\boldsymbol{F}_E=\left(\boldsymbol{J}^{\mathrm{T}}\right)^{+}\boldsymbol{F}$ as the effective forces of actuators and $\boldsymbol{f}_I=\left[\boldsymbol{I}-\left(\boldsymbol{J}^{\mathrm{T}}\right)^{+}\boldsymbol{J}^{\mathrm{T}}\right]\boldsymbol{f}$ as the internal force of actuators. $\boldsymbol{F}_E$ and $\boldsymbol{f}_I$ yield following equations:

$$\boldsymbol{J}^{\mathrm{T}}\boldsymbol{f}=\boldsymbol{J}^{\mathrm{T}}\boldsymbol{f}_E+\boldsymbol{J}^{\mathrm{T}}\boldsymbol{f}_I=\boldsymbol{J}^{\mathrm{T}}\boldsymbol{f}_E=\boldsymbol{F} \tag{7}$$

$$\boldsymbol{E}^{\mathrm{T}}\boldsymbol{f}=\boldsymbol{E}^{\mathrm{T}}\boldsymbol{f}_E+\boldsymbol{E}^{\mathrm{T}}\boldsymbol{f}_I=\boldsymbol{E}^{\mathrm{T}}\boldsymbol{f}_I=\boldsymbol{F}_r \tag{8}$$

where $\boldsymbol{F}_r$ is the 2×1 internal force vector.

2) CONTROL LOOP OF THE POSITION TRACKING

As shown in Fig. 5, the position control loop is used to control poses of the movement platform and a real-time kinematics solution is used to improve the precision of the control system. The feedback pose $\boldsymbol{q}$ of the movement platform is solved using the kinematic solution module according to current actuator length $\boldsymbol{l}$. By comparing the desired pose $\boldsymbol{q}_d$ with the feedback pose $\boldsymbol{q}$ of the movement platform, the pose error $\boldsymbol{e}_q$ is obtained. Then, the pose error is fed into the position PI controller to produce the DOF error control quantities. The control law could be expressed as following:

$$\boldsymbol{u}_q=\boldsymbol{k}_P\boldsymbol{e}_q+\boldsymbol{k}_I\int_0^t\boldsymbol{e}_q dt \tag{9}$$

where $\boldsymbol{k}_P$ and $\boldsymbol{k}_I$ are 6×6 diagonal gain matrix for proportional and integral part respectively.

Besides that, in order to increase the damping of hydraulic system, an acceleration feedback loop is introduced into the task space. The feedback pose acceleration $\ddot{\boldsymbol{q}}$ of the movement platform is solved according to the feedback acceleration $\boldsymbol{a}$ provided by eight acceleration sensors, and the control quantity $\boldsymbol{u}_a$ is obtained through the feedback proportional gain $\boldsymbol{k}_{af}$. By using Jacobian matrix $\boldsymbol{J}$, the position controller output is converted into hydraulic servo valve input $\boldsymbol{u}_p$. The control law of position control loop could be expressed as following:

$$\boldsymbol{u}_p=\boldsymbol{J}\left(\boldsymbol{u}_q-\boldsymbol{k}_{af}\ddot{\boldsymbol{q}}\right) \tag{10}$$

3) CONTROL LOOP OF THE INTERNAL FORCE SUPPRESSION

For the stiff platform, small errors in position measurement may lead to large internal forces, and the internal forces exert directly to the movement platform. Therefore, controlling force has more advantages than position in redundant DOF space.

According to equation (5), the internal force space changes with the platform position. Therefore, the internal force basis $\boldsymbol{E}$ is solved by using kinematic solution. The internal force suppression control loop is shown by Fig. 5. The feedback force $\boldsymbol{f}$ is convert into the 2×1 force vector $\boldsymbol{F}_r$ by using transpose of basis matrix $\boldsymbol{E}^{\mathrm{T}}$. $\boldsymbol{F}_r$ is compared with the desired force $\boldsymbol{F}_{rd}$ (normally be commanded to zero) and the

force errors are fed into the force controller. Then, the output of the force controller is converted into hydraulic servo valve input $\boldsymbol{u}_f$ by using the internal force basis matrix $\boldsymbol{E}$.

Combining with PI controller, the control law of internal force suppression can be expressed as following:

$$\boldsymbol{u}_f=-\boldsymbol{E}(\boldsymbol{k}_{fP}\boldsymbol{E}^{\mathrm{T}}\boldsymbol{f}+\boldsymbol{k}_{fI}\int_0^t\boldsymbol{E}^{\mathrm{T}}\boldsymbol{f}\,dt) \tag{11}$$

where $\boldsymbol{u}_f$ is the driving signal of hydraulic servo valve, $\boldsymbol{k}_{fP}$ and $\boldsymbol{k}_{fI}$ are 2×2 diagonal gain matrix for proportional and integral part, respectively.

4) INTEGRATED CONTROL

The integrated control strategy for redundancy shaking table is shown in Fig. 5. It is a hybrid position/force control scheme which comprises of a position tracking control loop and an internal force suppression control loop.

The position tracking control loop is used to control platform pose as requested in the task space. The internal force suppression control loop is used to eliminate the internal force caused by the movement of platform. The final servo valve input $\boldsymbol{u}$ is the sum of control quantities $\boldsymbol{u}_p$ and $\boldsymbol{u}_f$.

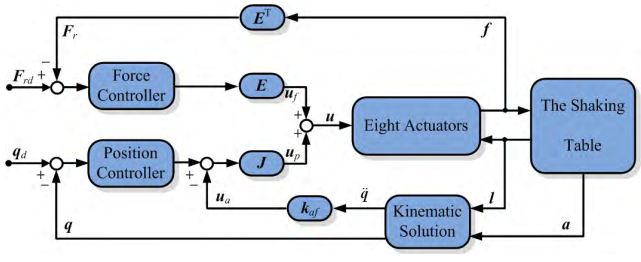

FIGURE 5. Integrated control block diagram for redundancy shaking table.

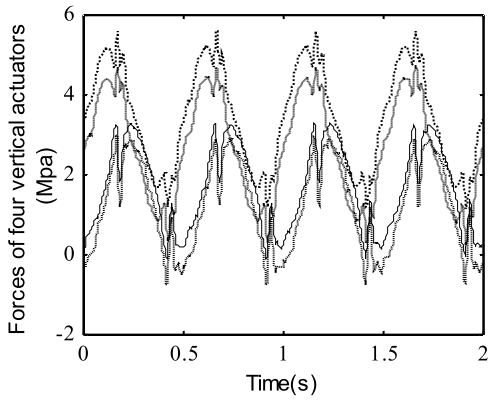

(a) Forces of four vertical actuators without internal force control.

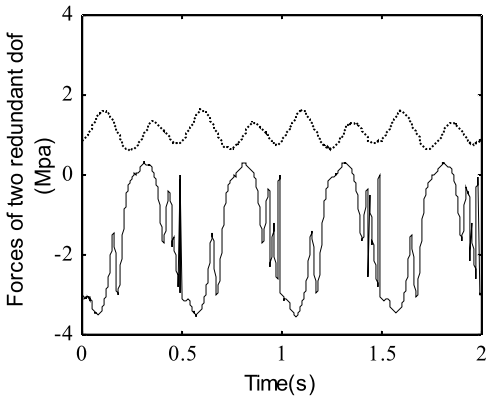

(b) Forces of two redundant DOFs without internal force control.

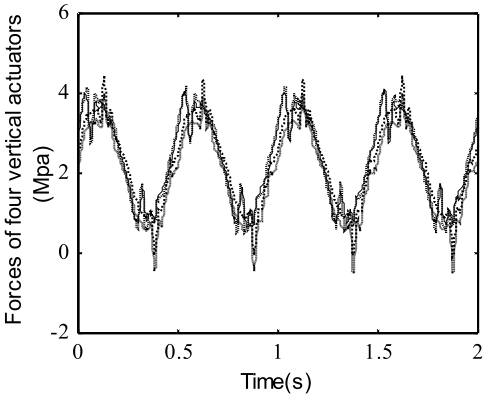

(c) Forces of four vertical actuators with internal force control.

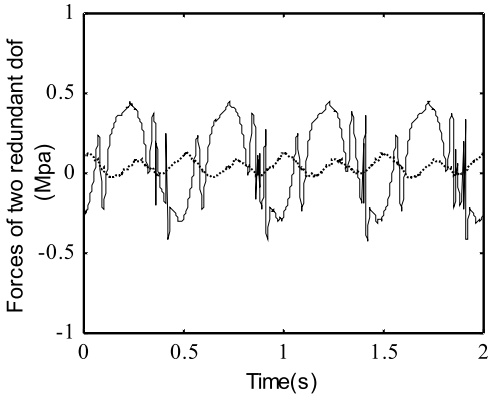

(d) Forces of two redundant DOFs with internal force control.

FIGURE 6. **Results of internal force rejection.**

C. EXPERIMENT AND RESULTS

In order to verify the effectiveness of the internal force suppression control scheme, a comparison experiment was carried out on HPM-2AR. In the experiment, the hydraulic power supply pressure was 28.0 Mpa. As mentioned in part A., there is no force sensor in the system. The system only has a differential pressure sensor for each hydraulic cylinder. Therefore, the force information of the system is indirectly evaluated through the differential pressure multiplied by the effective working area of hydraulic cylinder (0.0013 m^2). The desired forces of two redundant DOFs were both to zero. A sinusoidal motion command with amplitude of 60 mm and frequency of 2Hz was given to HPM-2AR in z direction. Initially, a pure position controller was attained for HPM-2AR by removing the internal force suppression control loop. Then, the control law of internal force suppression was applied with the same position loop settings as before and with the internal force suppression loop gain $\boldsymbol{k}_{fP} = \text{diag}\{2.0\ 2.0\}$ and $\boldsymbol{k}_{fI} = \text{diag}\{0.5\ 0.5\}$.

As shown in Fig. 6 (a), without the internal force control, the maximum thrust and tension of four vertical actuators were 5.5 Mpa and 0.8 Mpa, respectively. Besides that, the same side output forces of four vertical actuators were different because of the existence of large internal forces. Accordingly, the maximum force of two redundant DOFs was 3.5 Mpa which was shown by Fig. 6 (b). Moreover, the forces of two redundant DOFs both have offsets which arise from the null bias of servo valves.

After the internal force suppression control has been applied, the maximum thrust and tension of four vertical actuators were reduced to 4.4 Mpa and 0.4 Mpa respectively, as shown by Fig. 6(c). At the same time, the same side output forces of four vertical actuators were almost same. Accordingly, the maximum force of two redundant DOFs was reduced to smaller than 0.4 Mpa, as shown in Fig. 6 (d). The force offsets of two redundant DOFs were also eliminated through the integral element of internal force controller. The experiment results indicated that the internal force controller is effective to reduce the internal forces of HPM-2AR and increase the net force output of the system.

IV. AUTO-DOCKING MECHANISM

A. SYSTEM DESCRIPTION

Auto-docking is a typical interactive task for robots [26]. As shown in Fig. 7, the auto-docking mechanism composes of a 6-DOF HPM, the target object and a vision system. In the horizontally-mounted HPM, the hydraulic actuator consists of an asymmetric servo valve and an asymmetric

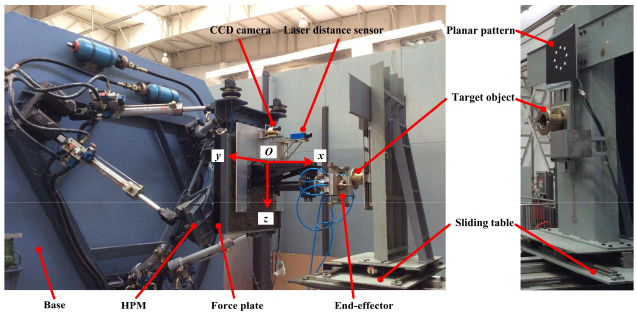

FIGURE 7. Auto-docking mechanism.

hydraulic cylinder with a built-in displacement sensor and two oil-pressure sensors. A force plate was installed between the supporting rack of the end-effector and the movement platform to obtain the contact force/torque. The target was installed on a sliding table and moves smoothly in x, y, and z directions with a wide range by using three stepping motors. To facilitate docking, two guide rods were installed on end-effector with two pin holes were punched in target. In order to obtain the relative pose of two interaction objects, the vision system was established which constituted of a CCD camera, a planar graph and a laser distance sensor.

B. SYSTEM FEATURES AND CONTROL SCHEME

The auto-docking mechanism has three significant features. First, the target object has large movement range and expects the relative position tracking as accurate as possible. Second, the contact forces between the end-effector and the target object should be well controlled to guarantee the safety of interaction tasks. Third, the end-effector is heavy.

In view of the first two features, the vision and force sensor should be integrated into the interaction control. The vision sensor provides the relative pose measurement between two interaction sides without direct physical contact and relaxes the exact positioning requirement for the end-effector. Besides that, the proximally located force sensor provides localized contact information to enhance the dexterity and safety of interaction task. Therefore, the compliant motion control is required. Accordingly, the hybrid impedance control scheme on the basis of vision and force was proposed in the paper. The control scheme has an inner and outer loop structure. On the basis of joint space control scheme, the inner loop control is devised to track pose commands from outer loop through tracking the length command of each actuator. The outer loop control is set up to determine the motion trajectory of the end-effector according to vision and force feedback and achieves the expected compliant docking behavior.

In view of the third feature, the docking mechanism should have enough stiffness. In consideration of high force capabilities of hydraulic parallel mechanisms, the 6-DOF hydraulic parallel mechanism is used to carry out auto-docking. However, the inherent nonlinearities and small damping characteristic of hydraulic servosystem are main challenges for

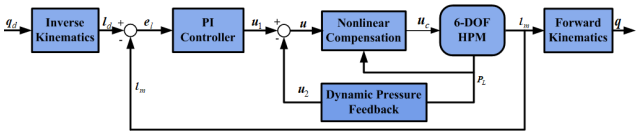

FIGURE 8. Block diagram of position control inner loop.

compliant motion control. In order to increase damping of hydraulic system, the dynamic pressure feedback is adopted by the inner control with the help of two oil-pressure sensors in each hydraulic actuator. Furthermore, a nonlinear compensation part is devised to overcome the negative impact of flow load sensitivity of hydraulic servo valve on control system.

1) INNER LOOP OF THE POSITION CONTROL

The position control inner loop is set up based on the joint space control scheme [22]. The block diagram of position control inner loop is shown in Fig. 8. It computes the actuator length command $\boldsymbol{l}_d$ at specific docking pose $\boldsymbol{q}_d$ by using inverse kinematics and realizes the position closed-loop through the built-in displacement sensor feedback of hydraulic cylinder. Besides that, the dynamic pressure feedback is introduced to increase the damping of system. Furthermore, a nonlinear compensation module is adopted to eliminate the impact of flow load sensitivity of hydraulic servo valve on control performance.

The dynamic pressure feedback $\boldsymbol{u}_2$ is given by:

$$\boldsymbol{u}_2 = \boldsymbol{k}_{fp} \frac{\boldsymbol{T}_p s}{\boldsymbol{T}_p s + 1} \boldsymbol{P}_L \tag{12}$$

where $\boldsymbol{k}_{fp}$ is the 6×6 diagonal gain matrix, $\boldsymbol{T}_p$ is the time constant, and $\boldsymbol{P}_L$ is the 6×1 load pressure vector.

$\boldsymbol{P}_L$ could be expressed as following:

$$\boldsymbol{P}_L = \boldsymbol{P}_1 - n_1 \boldsymbol{P}_2 \tag{13}$$

where $\boldsymbol{P}_1$ is the 6×1 pressure vector of the hydraulic cylinder rod side, $\boldsymbol{P}_2$ is the 6×1 pressure vector of the hydraulic cylinder piston side, and n_1 is the effective area ratio between the rod side and piston side.

In order to reduce the flow load sensitivity of hydraulic servo valve, a nonlinear compensation module is devised as following:

$$u_{cj} = \sqrt{p_s / \left(k_j p_s - sign\left(u_j\right) P_{Lj}\right)} u_j = h\left(P_{Lj}\right) u_j \tag{14}$$

where p_s is oil source pressure, k_i equals 1 when $u_i \geq 0$ and equals n_1 when $u_i < 0$, $sign(u_i)$ equals 1 when $u_i \geq 0$ and equals -1 when $u_i < 0$, and P_{Li} is the load pressure of the i-th hydraulic cylinder.

Combining with PI controller, the control law of inner loop is expressed by following:

$$\boldsymbol{u}_c = \boldsymbol{h}\left(\boldsymbol{P}_L\right)\left(\boldsymbol{k}_P \boldsymbol{e}_l + \boldsymbol{C}\boldsymbol{k}_I \int_0^t \boldsymbol{e}_l dt - \boldsymbol{u}_2\right) \tag{15}$$

where $\boldsymbol{k}_P$ and $\boldsymbol{k}_I$ are 6×6 diagonal gain matrix for proportional and integral part respectively, $\boldsymbol{e}_l$ is the actuator length error, and $\boldsymbol{u}_2$ is the dynamic pressure feedback.

2) OUTER LOOP OF THE COMPLIANT MOTION CONTROL

In order to obtain the force-controlled coordinate $\boldsymbol{Sq}$ and the position-controlled coordinate $\boldsymbol{(I\text{-}S)q}$, the working coordinate $\boldsymbol{q}$ is divided by the 6×6 diagonal selection matrix $\boldsymbol{S}$ [12]. The following control law can be derived for force-controlled coordinates with the PI force controller.

$$\boldsymbol{Sq}_d = \boldsymbol{Sq}_r + \boldsymbol{S}\left[\boldsymbol{k}_{FP}(\boldsymbol{F}_d - \boldsymbol{F}) + \boldsymbol{k}_{FI}\int_0^t (\boldsymbol{F}_d - \boldsymbol{F})dt\right] \quad (16)$$

where $\boldsymbol{F}_d$ and $\boldsymbol{F}$ are the desired and measured 6×1 contact force vector respectively, $\boldsymbol{k}_{FP}$ is the 6×6 diagonal proportional gain matrix, $\boldsymbol{k}_{FI}$ is the 6×6 diagonal integral gain matrix, $\boldsymbol{q}_d$ and $\boldsymbol{q}_r$ are the desired and reference 6×1 pose vector respectively, $\boldsymbol{Sq}_d$ and $\boldsymbol{Sq}_r$ are the divided force-controlled coordinate values for $\boldsymbol{q}_d$ and $\boldsymbol{q}_r$ respectively.

The reference pose vector $\boldsymbol{q}_r$ can be expressed as following:

$$\boldsymbol{q}_r = \boldsymbol{k}_{PI}\int_0^t (\boldsymbol{e}_{qd} - \boldsymbol{e}_q)dt \quad (17)$$

where $\boldsymbol{e}_{qd}$ and $\boldsymbol{e}_q$ are the desired and measured 6×1 relative pose vector respectively, $\boldsymbol{k}_{PI}$ is the 6×6 diagonal gain matrix.

The force control law is derived by substituting equation (17) into equation (16) and could be expressed as following:

$$\begin{aligned}\boldsymbol{Sq}_d = {} & \boldsymbol{S}\left[\boldsymbol{k}_{PI}\int_0^t (\boldsymbol{e}_{qd} - \boldsymbol{e}_q)dt\right] \\ & + \boldsymbol{S}\left[\boldsymbol{k}_{FP}(\boldsymbol{F}_d - \boldsymbol{F}) + \boldsymbol{k}_{FI}\int_0^t (\boldsymbol{F}_d - \boldsymbol{F})dt\right] \quad (18)\end{aligned}$$

For the position-controlled coordinate, the control law could be denoted as following:

$$(\boldsymbol{I} - \boldsymbol{S})\,\boldsymbol{q}_d = (\boldsymbol{I} - \boldsymbol{S})\,\boldsymbol{q}_r \quad (19)$$

Thus, the control law is obtained by summing equation (18) and equation (19) and expressed as following:

$$\begin{aligned}\boldsymbol{q}_d = {} & \boldsymbol{k}_{PI}\int_0^t (\boldsymbol{e}_{qd} - \boldsymbol{e}_q)dt \\ & + \boldsymbol{S}\left[\boldsymbol{k}_{FP}(\boldsymbol{F}_d - \boldsymbol{F}) + \boldsymbol{k}_{FI}\int_0^t (\boldsymbol{F}_d - \boldsymbol{F})dt\right] \quad (20)\end{aligned}$$

3) INTEGRATED CONTROL

The integrated control strategy for auto-docking mechanism is shown in Fig. 9. It is a hybrid impedance control scheme which comprises of a position tracking control inner loop and a compliant motion control outer loop. The position control inner loop tracks pose commands from outer loop as accuracy as possible and has fast response by high iteration rate (500 Hz). The compliant motion control outer loop outputs expected motion profile of the end-effector and achieves the expected compliant docking behavior according to vision and force feedback by iteration with relative lower sample rate (100 Hz).

Since the desired trajectories are required to be continuously revised according to real-time feedback of relative pose and contact force during docking. The task sequencer and trajectory generation component are additionally implemented by finite state machine of Simulink ®. During docking, obstacles may appear between the end-effector and the target object, or the motion amplitude and speed of the target object may exceed the normal docking range. For these cases, the trajectory generation module will suspend or slow down the moving of end-effector in z direction to prevent the damage of the mechanism.

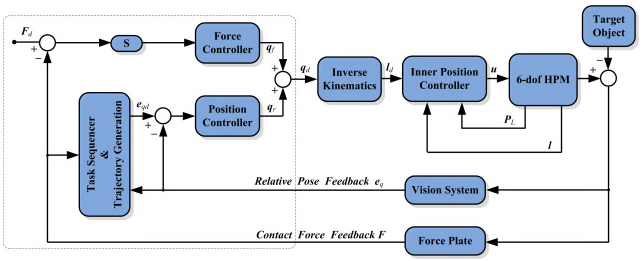

FIGURE 9. Integrated control block diagram for auto-docking mechanism.

C. EXPERIMENT AND RESULTS

A series of auto-docking dynamic experiments were carried out to verify the proposed control scheme. In the experiments, position control was adopted for all rotational DOFs and translational DOF in x direction. On the other hand, force control was adopted for other DOFs. The desired attitude angles in y direction and the desired contact forces in z direction were both set to zero. The move command for end-effector in x direction depends on relative positions of two interaction objects in y and z direction. Once the relative position errors in y and z direction within the particular range, the 6-DOF HPM would move forward to a specified value in x direction.

As shown in Fig. 10(a) by dashed lines, the experiment contains seven stages: (1) initialization, (2) retraction, (3) approaching, (4) contacting, (5) locked and tracking, (6) unlocked and return, and (7) finalization. At initialization time, the movement platform stayed at the relative zero position and the target object located at ($x = 133$ mm, $y = -26$ mm, $z = -93$ mm) in the inertial coordinate. Then, the target object was moving ± 100 mm along the y and z direction at the speed of $\pm$ 50mm/s and $\pm$ 40 mm/s, respectively. At the retraction stage, the relative position command was set to ($x = 300$ mm, $y = 0$ mm, $z = 0$ mm). Once the movement platform retracted to the specific location and the relative position errors in y and z direction were both less than 10 mm, the forward movement command in x direction was sent. Then, the end-effector was moving forward in x direction and tracking the target object in y and z direction until 51 s. During contacting, the poses of the end-effector were continuously adjusted to achieve the compliant contact. Once the end-effector and the target object were fully contact, they were locked together. Thereafter, the 6-DOF HPM was tracing the target object until return command was sent

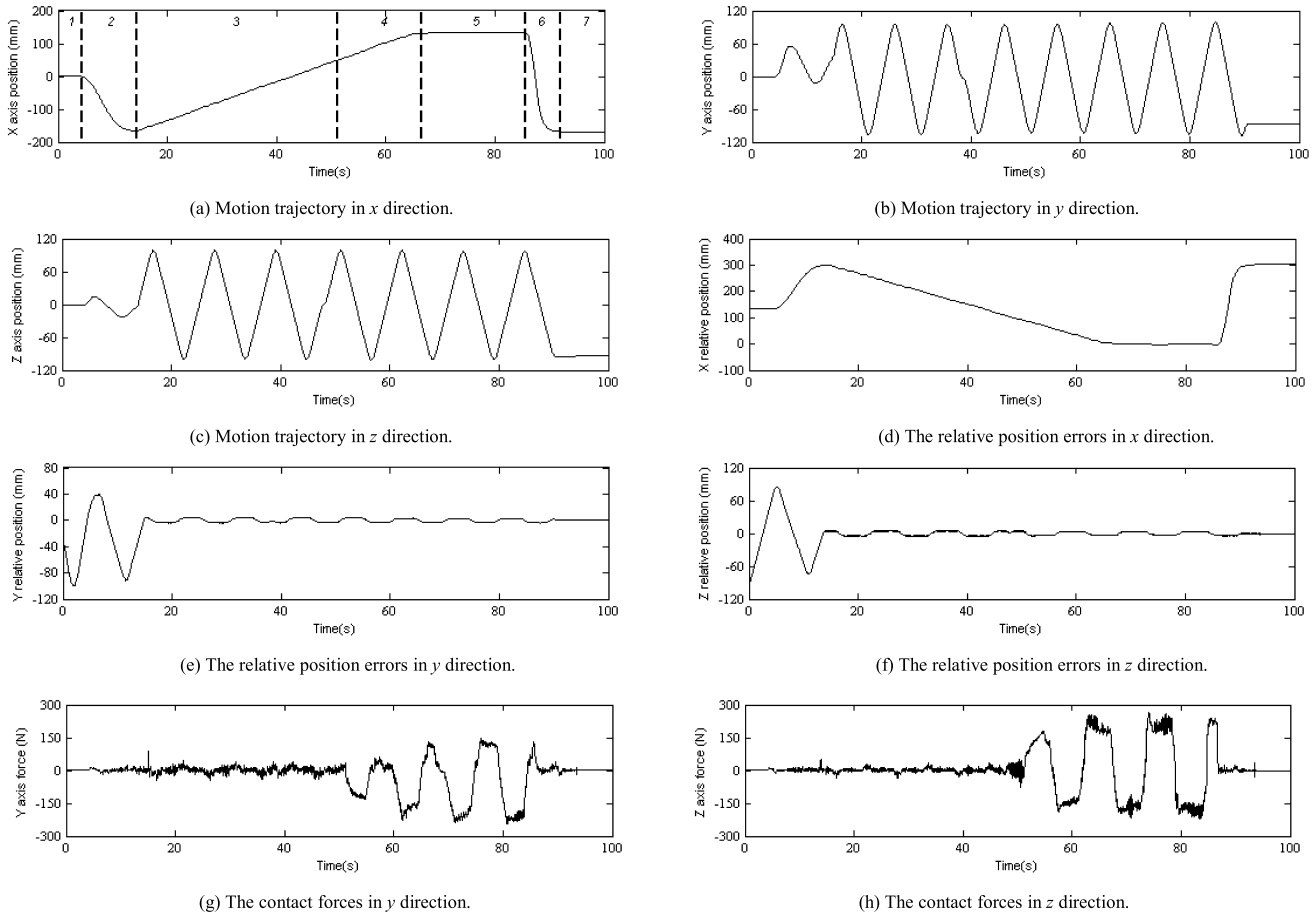

(a) Motion trajectory in x direction.

(b) Motion trajectory in y direction.

(c) Motion trajectory in z direction.

(d) The relative position errors in x direction.

(e) The relative position errors in y direction.

(f) The relative position errors in z direction.

(g) The contact forces in y direction.

(h) The contact forces in z direction.

FIGURE 10. **Auto-docking dynamic experiment.**

at 85s. Finally, the end-effector released the target object and returned to 300 mm in x direction.

As can be seen from Fig. 10(b), Fig. 10(c), Fig. 10(e) and Fig. 10(f), when the end-effector was approaching the target object, the generated motion trajectory in y and z direction were smooth and the relative position errors were always lower than 10 mm. When the end-effector was contacting, locked and tracking the target object, the contact forces in y and z direction were well controlled below 300 N (lower than the contact force limitation of maximum 1000 N), as can be seen from Fig. 10(g) and Fig. 10(h). These results showed that the hybrid impedance control scheme proposed by this paper achieved fast and accurate tracking to the target object with high flexibility and had good compliant control effect which is appropriate for the interaction task under uncertain environment.

V. CONCLUSION

In this paper, compliant control techniques for 6-DOF HPM have been investigated and implemented. According to the specifications of manipulation task and the features of mechanism, three different compliant motion control schemes were presented in three application scenarios, respectively: a parallel position/force control scheme in the joint space for the train curve negotiation performance test, a hybrid position/force control scheme for internal force suppression of shaking table with actuation redundancy, and a hybrid impedance control scheme for auto-docking mechanism on the basis of vision and force servo. In addition, improved methods have also been taken to increase the damping and counteract the disadvantageous influences of nonlinearities in hydraulic servosystem. The feasibility and effectiveness of the proposed schemes were verified through a series of experiments. These schemes could be applied to other application fields as references where the compliant behavior of manipulator using the 6-DOF HPM is required. However, some complex interaction tasks may arise more challenging problems, such as unknown parameters, unstructured environments or external disturbances, the stability and stabilization, etc. In these cases, the control schemes presented in this paper may not enough, some more advanced control techniques such as adaptive fuzzy control [13], [14], adaptive neural output-feedback control for the nonlinear system with unmodeled dynamics [15], robust control [27], H_∞ control [28], and the effective methods for improving system stability [29], [30], etc. need to be considered.

REFERENCES

[1] L.-W. Tsai, *Robot Analysis: The Mechanics of Serial and Parallel Manipulators*. Hoboken, NJ, USA: Wiley, 1999.
[2] M. Namvar and F. Aghili, "Adaptive force-motion control of coordinated robots interacting with geometrically unknown environments," *IEEE Trans. Robot.*, vol. 21, no. 4, pp. 678–694, Aug. 2005.
[3] A. Stolt, A. Robertsson, and R. Johansson, "Robotic force estimation using dithering to decrease the low velocity friction uncertainties," in *Proc. Int. Conf. Robot. Autom. (ICRA)*, May 2015, pp. 3896–3902.
[4] J. D. Schutter and H. Van Brussel, "Compliant robot motion II. A control approach based on external control loops," *Int. J. Robot Res.*, vol. 7, no. 4, pp. 18–33, 1988.
[5] D. E. Whitney, "Historical perspective and state of the art in robot force control," in *Proc. Int. Conf. Robot. Autom. (ICRA)*, Apr. 2003, pp. 269–274.
[6] G. Zeng and A. Hemami, "An overview of robot force control," *Robotica*, vol. 15, no. 4, pp. 473–482, 1997.
[7] N. Hogan, "Impedance control: An approach to manipulation: Part II—Implementation," *J. Dyn. Syst. Meas. Control.*, vol. 107, no. 1, pp. 8–16, 1985.
[8] M. T. Mason, "Compliance and force control for computer controlled manipulators," *IEEE Trans. Syst., Man, Cybern.*, vol. SMC-11, no. 6, pp. 418–432, Jun. 1981.
[9] S. Chiaverini and L. Sciavicco, "The parallel approach to force/position control of robotic manipulators," *IEEE Trans. Robot. Autom.*, vol. 9, no. 4, pp. 361–373, Aug. 1993.
[10] S. Chiaverini, B. Siciliano, and L. Villani, "A survey of robot interaction control schemes with experimental comparison," *IEEE/ASME Trans. Mechatronics*, vol. 4, no. 3, pp. 273–285, Sep. 1999.
[11] M. Pelletier and M. Doyon, "On the implementation and performance of impedance control on position controlled robots," in *Proc. Int. Conf. Robot. Autom. (ICRA)*, May 1994, pp. 96–102.
[12] R. Anderson and M. W. Spong, "Hybrid impedance control of robotic manipulators," *IEEE J. Robot. Autom.*, vol. 4, no. 5, pp. 549–556, Oct. 1988.
[13] X. Zhao, P. Shi, and X. Zheng, "Fuzzy adaptive control design and discretization for a class of nonlinear uncertain systems," *IEEE Trans. Cybern.*, vol. 46, no. 6, pp. 1476–1483, Jun. 2016.
[14] X. Huo, L. Ma, X. Zhao, and G. Zong, "Observer-based fuzzy adaptive stabilization of uncertain switched stochastic nonlinear systems with input quantization," *J. Franklin Inst.*, vol. 356, no. 4, pp. 1789–1809, 2019.
[15] H. Wang, P. X. Liu, S. Li, and D. Wang, "Adaptive neural output-feedback control for a class of nonlower triangular nonlinear systems with unmodeled dynamics," *IEEE Trans. Neural Netw. Learn. Syst.*, vol. 29, no. 8, pp. 3658–3668, Aug. 2018.
[16] M. R. C. Qazani, S. Pedrammehr, A. Rahmani, B. Danaei, M. M. Ettefagh, A. K. S. Rajab, and H. Abdi, "Kinematic analysis and workspace determination of hexarot-a novel 6-DOF parallel manipulator with a rotation-symmetric arm system," *Robotica*, vol. 33, pp. 1686–1703, Oct. 2015.
[17] A. M. Lopes and F. G. Almeida, "Acceleration based force-impedance control of a 6-dof parallel robotic manipulator," in *Proc. Int. Conf. Comput. Cybern.*, Aug. 2006, pp. 1–6.
[18] G. Liu, Z. Qu, X. Liu, and J. Han, "Tracking performance improvements of an electrohydraulic Gough–Stewart platform using a fuzzy incremental controller," *Ind. Robot Int. J.*, vol. 41, no. 2, pp. 225–235, 2014.
[19] Z. Zyada, Y. Hasegawa, and T. Fukuda, "Multi-directional assembly of tunnel segments using a force controlled parallel link robot with fuzzy compensation," in *Proc. SICE Annu. Conf.*, Aug. 2003, pp. 2044–2049.
[20] H. Seraji and A. Howard, "Behavior-based robot navigation on challenging terrain: A fuzzy logic approach," *IEEE Trans. Robot. Autom.*, vol. 18, no. 3, pp. 308–321, Jun. 2002.
[21] T. K. Bera, R. Merzouki, B. O. Bouamama, and A. K. Samantaray, "Force control in a parallel manipulator through virtual foundations," *Proc. Inst. Mech. Eng., I, J. Syst. Control Eng.*, vol. 226, no. 8, pp. 1088–1106, 2012.
[22] B. Siciliano, L. Sciavicco, L. Villani, and G. Oriolo, *Robotics: Modelling, Planning and Control*. New York, NY, USA: Springer-Verlag, 2010.
[23] N. D. Manring, *Hydraulic Control Systems*. Hoboken, NJ, USA: Wiley, 2005.
[24] G. Lee, J. I. Jeong, and J. Kim, "Calibration of encoder indexing of a redundantly actuated parallel mechanism to eliminate contradicting control forces," *Mech. Based Des. Struct. Mach.*, vol. 44, no. 4, pp. 306–316, 2016.
[25] A. Plummer, "A general co-ordinate transformation framework for multi-axis motion control with applications in the testing industry," *Control Eng. Pract.*, vol. 18, no. 6, pp. 598–607, 2010.
[26] A. Weiss, M. Baldwin, R. S. Erwin, and I. Kolmanovsky, "Model predictive control for spacecraft rendezvous and docking: Strategies for handling constraints and case studies," *IEEE Trans. Control Syst. Technol.*, vol. 23, no. 4, pp. 1638–1647, Jul. 2015.
[27] H. Wang, P. X. Liu, and B. Niu, "Robust fuzzy adaptive tracking control for nonaffine stochastic nonlinear switching systems," *IEEE Trans. Cybern.*, vol. 48, no. 8, pp. 2462–2471, Aug. 2018.
[28] X.-H. Chang and G.-H. Yang, "New results on output feedback H_∞ control for linear discrete-time systems," *IEEE Trans. Autom. Control.*, vol. 59, no. 5, pp. 1355–1359, May 2014.
[29] Y. Yin, G. Zong, and X. Zhao, "Improved stability criteria for switched positive linear systems with average dwell time switching," *J. Franklin Inst.*, vol. 354, no. 8, pp. 3472–3484, May 2017.
[30] Y. Yin, X. Zhao, and X. Zheng, "New stability and stabilization conditions of switched systems with mode-dependent average dwell time," *Circuits Syst. Signal Process.*, vol. 36, no. 1, pp. 82–98, 2017.
[31] C. Gao, S. Zheng, D. Cong, J. Han, Z. Yang, and J. Sun, "Modeling and control of the CSCEC multi-function testing system," *J. Earthq. Eng.*, vol. 22, no. 2, pp. 257–280, 2018.

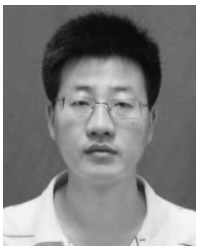

SHUPENG ZHENG received the M.S. degree in computer science and the Ph.D. degree in mechatronics engineering from the Harbin Institute of Technology, Harbin, China, in 2006 and 2011, respectively. He is currently a Lecturer with the School of Electrical and Information, Northeast Agricultural University, Harbin. His research interests include electric-hydraulic servo control, real-time control systems, embedded computing, and multi-mode controller design.

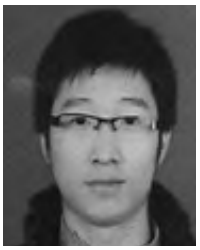

CHANGHONG GAO received the M.S. degree in mechanical engineering from the Lanzhou University of Technology, Lanzhou, China, in 2012, and the Ph.D. degree in mechatronics engineering from the Harbin Institute of Technology, Harbin, China, in 2017. He is currently a Senior Engineer with the Aviation Equipment Research Institute, AVIC Qing'an Group Company Ltd., Xi'an, China. His research interests include load simulation, motion simulator, mechatronic systems and servo control, adaptive robust control, and sliding mode control.

INJIAN NIU received the B.E. degree in mechatronics engineering from the Anhui University of Technology, Maanshan, China, in 2012, and the M.S. degree in mechatronics engineering from the Harbin Institute of Technology, Harbin, China, in 2014, where he is currently pursuing the Ph.D. degree. His research interests include electric-hydraulic servo control, scoliosis brace systems, parallel manipulator control, modal space active force control, and PD control with DGC.

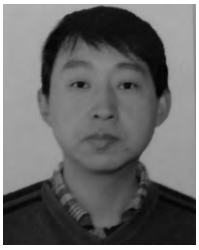

DACHENG CONG received the Ph.D. degree in instrument science and technology from the Harbin Institute of Technology, Harbin, China, in 2002, where he was an Associate Professor with the Department of Mechatronics Engineering, since 2003, and has also been a Professor, since 2008. He has authored or coauthored more than 50 journals and conference articles. His current research interests include 6-DOF shaking table's vibration control, 6-DOF motion simulation control systems, and three-stage servo valve control technique with large flow and high response. He is a member of the Fluid Power Transmission and Control Association and the China Ordnance Society.

JUNWEI HAN received the Ph.D. degree in mechatronics engineering degree from the Harbin Institute of Technology, Harbin, China, in 1992, where he has been a Professor with the Department of Mechatronics Engineering, since 1997. He is currently an Academic Leader of fluid power transmission and control and the Director of the Institute of Simulation and Test of Electro-Hydraulic Servo System, and the National State Key Laboratory of Robotics and System. He has authored or coauthored more than 180 journals and conference articles. He honored the ministry of education in the new century excellent talents and the defense industry young and middle-aged expert with outstanding contributions. His current research interests include electro-hydraulic servo control, redundant-driven parallel control, and flight simulation and simulation test systems, 6-DOF shaking table's vibration control, 6-DOF motion simulation control systems, and three-stage servo valve control technique with large flow and high response. He is a member of the Fluid Power Transmission and Control Association, and a Council Member of the China Ordnance Society.